Journal of Zhejiang University-SCIENCE A (Applied Physics & Engineering)
ISSN 1673-565X (Print); ISSN 1862-1775 (Online)
www.zju.edu.cn/jzus; www.springerlink.com
E-mail: jzus@zju.edu.cn

A 2.5D finite element approach for predicting ground vibrations generated by vertical track irregularities*

Xue-cheng BIAN†, Chang CHAO, Wan-feng JIN, Yun-min CHEN†‡

(*MOE Key Laboratory of Soft Soils and Geoenvironmental Engineering, Department of Civil Engineering, Zhejiang University, Hangzhou 310058, China*)

†E-mail: bianxc@zju.edu.cn; chenyunmin@zju.edu.cn

Received Sept. 23, 2011; Revision accepted Sept. 24, 2011; Crosschecked Sept. 24, 2011

Abstract: Dynamic responses of track structure and wave propagation in nearby ground vibration become significant when train operates on high speeds. A train-track-ground dynamic interaction analysis model based on the 2.5D finite element method is developed for the prediction of ground vibrations due to vertical track irregularities. The one-quarter car model is used to represent the train as lumped masses connected by springs. The embankment and the underlying ground are modeled by the 2.5D finite element approach to improve the computation efficiency. The Fourier transform is applied in the direction of train's movement to express the wave motion with a wave-number. The one-quarter car model is coupled into the global stiffness matrix describing the track-ground dynamic system with the displacement compatibility condition at the wheel-rail interface, including the irregularities on the track surface. Dynamic responses of the track and ground due to train's moving loads are obtained in the wave-number domain by solving the governing equation, using a conventional finite element procedure. The amplitude and wavelength are identified as two major parameters describing track irregularities. The irregularity amplitude has a direct impact on the vertical response for low-speed trains, both for short wavelength and long wavelength irregularities. Track irregularity with shorter wavelength can generate stronger track vibration both for low-speed and high-speed cases. For low-speed case, vibrations induced by track irregularities dominate far field responses. For high-speed case, the wavelength of track irregularities has very little effect on ground vibration at distances far from track center, and train's wheel axle weights becomes dominant.

Key words: High-speed railway, 2.5D finite element method, One-quarter car model, Ground vibration, Track irregularities
doi:10.1631/jzus.A11GT012 **Document code:** A **CLC number:** U213.1

1 Introduction

High-speed railway lines inevitably pass through densely populated urban areas. Train-induced environmental vibrations have received widely-expressed concerns from residents and railway constructors.

The load acting on railway track generally can be regarded as a combination of the moving quasi-static load and dynamic excitation (Sheng *et al*., 2003; Auersch, 2005; Lombaert and Degrande, 2009). The dynamic excitation comes from several sources, such as a parametric excitation due to the discrete supports of the rails, a transient excitation due to the rail joints and wheel flats, and the excitation due to wheel and rail roughness and track unevenness (Heckl *et al.*, 1996; Sheng *et al.*, 2003).

Vibrations induced by a moving quasi-static load have been extensively studied. A prediction model for ground vibration, coupling the quasi-static force and the Green function of a half-space, was proposed by Krylov (1995). Vibration induced by a constant or

‡ Corresponding author

* Project supported by the National Key Technology R&D Program of the Ministry of Science and Technology of China (No. 2009BAG12A01-B12-3), the National Natural Science Foundation of China (No. 51178418), and the Technology Promotion Program from the Ministry of Railway of China (No. 2008G005-D)

harmonic load moving along a beam resting on layered half-space is presented by Sheng *et al*. (1999a; 1999b) using an analytical solution. However, the existing model with a moving quasi-static load underestimates the actual response intensities of the railway structure and underlying ground, especially for higher excitation frequencies (Katou *et al*., 2008). Train wheel axle weights are also not the main factor in generating mid-frequency bands in the far field (Degrande and Lombaert, 2001; Takemiya and Bian, 2005). The train-track-ground dynamics interaction analysis indicates that the dynamic force generated at the wheel-rail contact cannot be ignored for evaluating ground vibration (Adolfsson *et al.*, 1999; Sheng *et al.*, 2003; 2004). For train travels at speeds below the velocity of wave propagation in the ground, the dynamic excitation is more important than the quasi-static axle loads for the generation of environmental vibration. When train's speed approaches or exceeds the Rayleigh wave velocity in the soil, the quasi-static excitation mechanism dominates the soil response (Galvin, 2010a).

Most aforementioned works use analytical solutions to express ground vibration due to moving loads. Although analytical solutions can help us understand the vibration generation mechanism due to traffic loadings, they cannot deal with complex track structures and the railway foundation. Rigueiro *et al.* (2010) concluded from theoretical analysis and experimental verification that a train-track dynamic interaction model is more reasonable than a moving force model for accessing vibration of ballasted track structure. A 3D multi-body and finite element-boundary element coupled model was presented by Galvin and Dominguez (2007) to predict vibrations in the time domain, considering the dynamic interaction between train and track.

The literature survey shows that dynamic excitation due to a train running on track with irregularities is essential to the evaluation of train traffic-induced environment vibration.

As an alternative to full 3D finite element models, the so-called 2.5D models have been proposed for the prediction of railway-induced ground vibrations (Yang and Hung, 2001; Takemiya, 2003; Bian *et al.*, 2008; Galvin, 2010b). This method effectively reduces the computational efforts and storage requirements.

In this paper, first, the essential procedures used in establishing the governing equations in terms of 2.5D finite elements are summarized. Then, the one-quarter car model and the harmonic track irregularity are combined to derive the dynamic excitation on track. The vehicle stiffness matrix describing the train motions will be coupled into the 2.5D finite element model for track and ground in the wave-number domain. Some computation results will be presented to discuss the effect of train speed and track irregularities on ground vibration.

2 2.5D finite element method

In this section, the major steps to derive a 2.5D finite element model will be briefly introduced. Since the material and geometry of track structure and its supporting ground can be regarded as constant in the direction of the train's movement, the Fourier transform with respect space coordinate in this direction is applied to simplify the 3D problem. If we assume the train runs in the x-direction, the Fourier transform with respect to x coordinate is defined as

$$u^x(\xi_x)=\int_{-\infty}^{+\infty}u(x)\exp(\mathrm{i}\xi_x x)\mathrm{d}x, \tag{1}$$

and its corresponding inverse transform is given by

$$u(x)=\frac{1}{2\pi}\int_{-\infty}^{+\infty}u^x(\xi_x)\exp(-\mathrm{i}\xi_x x)\mathrm{d}\xi_x, \tag{2}$$

where the variable with superscript 'x' represents the components in the wave-number domain. ξ_x is the x-directional wave-number.

The 2.5D finite element model of track-ground system is shown in Fig. 1. Double wheel loads $q(t)$ move in track's direction.

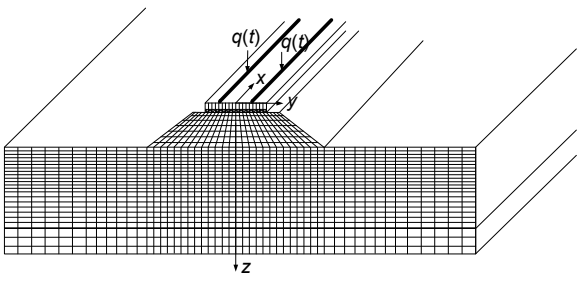

Fig. 1 2.5D finite element model of track-ground system

The motions of ground with homogeneous and isotropic material assumptions can be described by Navier's equations in the frequency domain:

$$\mu^* u^t_{i,jj} + (\lambda^* + \mu^*) u^t_{j,ji} + \omega^2 \rho u^t_i + f^t_i = 0, \quad (3)$$

where ω is the excitation frequency, ρ is the material's density, and λ and μ are Lame constants. In this study, the complex Lame constants λ^*, μ^* are used to consider the damping effect of wave propagation in ground, $\lambda^*=(1+2i\beta)\lambda$, $\mu^*=(1+2i\beta)\mu$, where β is the damping ratio of ground soil. Variables with superscript 't' represent the components in the frequency domain.

Strain components of an element can be given in the light of the small strain assumption. The predefined Fourier transform in x-direction is applied and yields the expressions in the wave-number domain:

$$\begin{aligned}
&\varepsilon^{xt}_{xx} = -\mathrm{i}\xi_x u^{xt},\ \gamma^{xt}_{xy} = -\mathrm{i}\xi_x v^{xt} + \frac{\partial u^{xt}}{\partial y},\\
&\varepsilon^{xt}_{yy} = \frac{\partial v^{xt}}{\partial y},\ \gamma^{xt}_{yz} = \frac{\partial w^{xt}}{\partial y} + \frac{\partial v^{xt}}{\partial z},\\
&\varepsilon^{xt}_{zz} = \frac{\partial w^{xt}}{\partial z},\ \gamma^{xt}_{zx} = \frac{\partial u^{xt}}{\partial z} - \mathrm{i}\,\xi_x w^{xt}.
\end{aligned} \quad (4)$$

Consequently, the strain-displacement relationship in the frequency and wave-number domain can be expressed by

$$\boldsymbol{\varepsilon}^{xt} = \boldsymbol{B}\boldsymbol{u}^{xt}, \quad (5)$$

where $\boldsymbol{\varepsilon}^{xt}$ and $\boldsymbol{u}^{xt}$ are the strain vector and displacement vector of the element, respectively, and their detailed expressions are given as below:

$$\boldsymbol{B} = \begin{bmatrix} -\mathrm{i}\xi_x & 0 & 0 & \dfrac{\partial}{\partial y} & 0 & \dfrac{\partial}{\partial z} \\ 0 & \dfrac{\partial}{\partial y} & 0 & -\mathrm{i}\xi_x & \dfrac{\partial}{\partial z} & 0 \\ 0 & 0 & \dfrac{\partial}{\partial z} & 0 & \dfrac{\partial}{\partial y} & -\mathrm{i}\xi_x \end{bmatrix}^{\mathrm{T}},$$

$$\boldsymbol{\varepsilon}^{xt} = \begin{bmatrix} \varepsilon^{xt}_{xx} & \varepsilon^{xt}_{yy} & \varepsilon^{xt}_{zz} & \gamma^{xt}_{xy} & \gamma^{xt}_{yz} & \gamma^{xt}_{zx} \end{bmatrix}^{\mathrm{T}},$$

$$\boldsymbol{u}^{xt} = \begin{bmatrix} u^{xt} & v^{xt} & w^{xt} \end{bmatrix}^{\mathrm{T}}. \quad (6)$$

In addition, the stress-strain relationship can be given by

$$\boldsymbol{\sigma}^{xt} = \boldsymbol{D}\varepsilon^{xt}, \quad (7)$$

where $\boldsymbol{\sigma}^{xt}$ is the stress vector of the element, and $\boldsymbol{D}$ is the elastic matrix:

$$\boldsymbol{D} = \begin{bmatrix} \lambda^*+2\mu^* & \lambda^* & \lambda^* & 0 & 0 & 0 \\ & \lambda^*+2\mu^* & \lambda^* & 0 & 0 & 0 \\ & & \lambda^*+2\mu^* & 0 & 0 & 0 \\ & & & \mu^* & 0 & 0 \\ & \text{sym} & & & \mu^* & 0 \\ & & & & & \mu^* \end{bmatrix}. \quad (8)$$

Since the $\boldsymbol{D}$ matrix is symmetric, only its upper part is given in Eq. (8). The ground is modeled by the quadrilateral element in such a way that the transversal vertical section is meshed by the finite elements, whose nodal displacements are defined in three degrees of freedom. A quadrilateral element with either four or eight nodes can be used to discretize the near field of track and ground. By introducing the shape function $\boldsymbol{N}$, the discretized form of the governing equation in the frequency domain can be derived by the conventional finite element method.

$$\left(\boldsymbol{K}^{xt} - \omega^2 \boldsymbol{M}\right)\boldsymbol{U}^{xt} = \boldsymbol{F}^{xt}, \quad (9)$$

where $\boldsymbol{U}^{xt}$ is the displacement vector in frequency and wave-number domain, and $\boldsymbol{M}$, $\boldsymbol{K}^{xt}$, $\boldsymbol{F}^{xt}$ are the mass matrix, stiffness matrix, and equivalent nodal force vector, respectively, and their detailed expressions are

$$\boldsymbol{M} = \sum_e \rho \iint \boldsymbol{N}^{\mathrm{T}} \boldsymbol{N} |\boldsymbol{J}| \mathrm{d}\eta \mathrm{d}\zeta, \quad (10a)$$

$$\boldsymbol{K}^{xt} = \sum_e \rho \iint \left(\boldsymbol{B}^* \boldsymbol{N}\right)^{\mathrm{T}} \boldsymbol{D}\left(\boldsymbol{B}\boldsymbol{N}\right) |\boldsymbol{J}| \mathrm{d}\eta \mathrm{d}\zeta, \quad (10b)$$

$$\boldsymbol{F}^{xt} = \sum_e \iint \boldsymbol{N}^{\mathrm{T}} \boldsymbol{f} |\boldsymbol{J}| \mathrm{d}\eta \mathrm{d}\zeta, \quad (10c)$$

where η and ζ are element's local coordinates, and 'e' represents element-wise integration, f is the external load acting on this element. $\boldsymbol{J}$ is the Jacobi matrix, and $|\boldsymbol{J}|$ is the corresponding determinant, $|\boldsymbol{J}|=\det\boldsymbol{J}$.

The 2.5D finite element method described here has been implemented into the computation code TRAVIB. Since the finite element itself cannot deal with the unbounded soil medium directly, because of the element size, an appropriate boundary must be constructed to prevent wave reflection back into the near field at the edge of the finite element zone. In this study, a frequency-dependent dashpot with viscous components normal and tangent to a given boundary is introduced to simulate the infinity of the ground (Bian *et al*., 2008).

3 Mathematical model of train running on track with harmonic irregularities

Fig. 2 shows the one-quarter car model to represent the train. In the model, k_p, c_p represent the stiffness and damping of the primary suspension, and k_s, c_s represent the stiffness and damping of the secondary suspension. The masses of the car body, the bogie and the wheel-sets are represented by $m_c/4$, $m_b/2$ and m_w, respectively. Since the bogie is supported by two wheel axles, one axle shares one half of the total bogie weight. The primary suspension connects the wheels to the bogie, therefore, k_p, c_p represent two times the total primary vertical stiffness and viscous damping. The car body is supported by two bogies and every axle carries one quarter of the car body mass, $m_c/4$. k_s and c_s *r*epresent one half of the secondary vertical stiffness and viscous damping, respectively. The train is supposed to move in track's direction at speed c. The vertical movements of car body, bogie, and wheels are represented by u_c, u_b, and u_w, respectively. The irregularities at rail surface are defined as a cosine distribution with amplitude A_r and wavelength L.

The equilibrium equation of the one-quarter car model can be written as

$$\begin{pmatrix} 0.25m_c & 0 & 0 \\ 0 & 0.5m_b & 0 \\ 0 & 0 & m_w \end{pmatrix}\begin{pmatrix} \ddot{u}_c(t) \\ \ddot{u}_b(t) \\ \ddot{u}_w(t) \end{pmatrix}+\begin{pmatrix} c_s & -c_s & 0 \\ -c_s & c_p+c_s & -c_p \\ 0 & -c_p & c_p \end{pmatrix}\begin{pmatrix} \dot{u}_c(t) \\ \dot{u}_b(t) \\ \dot{u}_w(t) \end{pmatrix}+\begin{pmatrix} k_s & -k_s & 0 \\ -k_s & k_p+k_s & -k_p \\ 0 & -k_p & k_p \end{pmatrix}\begin{pmatrix} u_c(t) \\ u_b(t) \\ u_w(t) \end{pmatrix}=\begin{pmatrix} 0.25m_c g \\ 0.50m_b g \\ m_w g-q(t) \end{pmatrix}. \quad (11)$$

By applying the Fourier transform with respect to time t to Eq. (11), we obtain the interaction forces $q(t)$ in the frequency domain $q(w)$, which can be re-arranged as follows:

$$\tilde{q}(\omega)=W_1\delta(\omega)+W_2\delta(\omega-\omega_r)+W_3\delta(\omega+\omega_r), \quad (12)$$

where $\omega_r=2\pi c/L$, $\omega_1=0$, $\omega_2=\omega_r$, $\omega_3=-\omega_r$, W_1, W_2, and W_3 can be expressed as

$$W_1=m_w g+0.5m_b g+0.25m_c g,$$

$$W_2=\frac{A_r}{2}\cdot\frac{-\omega_r^2L_1-i\omega_r^3L_2+\omega_r^4L_3+i\omega_r^5L_4-\omega_r^6L_5}{L_6+i\omega_rL_7-\omega_r^2L_8-i\omega_r^3L_9+\omega_r^4L_{10}},$$

$$W_3=\frac{A_r}{2}\cdot\frac{-\omega_r^2L_1+i\omega_r^3L_2+\omega_r^4L_3-i\omega_r^5L_4-\omega_r^6L_5}{L_6-i\omega_rL_7-\omega_r^2L_8+i\omega_r^3L_9+\omega_r^4L_{10}},$$

where

$$L_1=k_sk_p(m_w g+0.5m_b g+0.25m_c g),$$

$$L_2=(c_pk_s+k_pc_s)(m_w g+0.5m_b g+0.25m_c g),$$

$$L_3=c_sc_p(m_w g+0.5m_b g+0.25m_c g)+k_s(0.25m_cm_w+0.5m_bm_w)+k_p(0.125m_cm_b+0.25m_cm_w),$$

$$L_4=c_s(0.25m_cm_w+0.5m_bm_w)+c_p(0.125m_cm_b+0.25m_cm_w),$$

$$L_5=0.125m_cm_bm_w,$$

$$L_6=k_sk_p,$$

$$L_7=c_pk_s+k_pc_s,$$

$$L_8=c_sc_p+0.25(k_s+k_p)m_c+0.5m_bk_s,$$

$$L_9=0.25(c_s+c_p)m_c+0.5m_bc_s,$$

$$L_{10}=0.125m_cm_b.$$

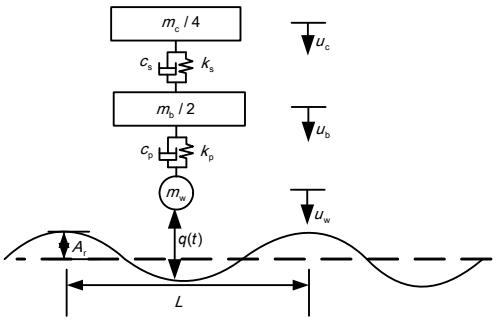

Fig. 2 One-quarter car model

For the train traveling at speed c on the track, the interaction forces in the frequency domain can be written as

$$\begin{aligned}\tilde{q}(\omega-\xi_x c) &= W_1\delta(\omega-\xi_x c)+W_2\delta(\omega-\omega_r-\xi_x c)\\ &\quad +W_3\delta(\omega+\omega_r-\xi_x c)\\ &= \frac{1}{c}\sum_{i=1}^{3}W_i\delta\left(\xi_x+\frac{\omega-\omega_i}{c}\right).\end{aligned} \tag{13}$$

Eq. (13) provides the dynamic loading due to a one-quarter car running at track with irregularities and can be readily coupled into Eq. (11).

4 Numerical results and discussion

To demonstrate the application of the proposed computation approach for the prediction of train-induced track and ground vibrations, a typical high-speed railway is adopted in the numerical computation. The mass of double rails per unit length is 120 kg/m. The bending stiffness of rail is 1.26×10^7 N·m^2, and its loss factor is 0.01. A simplified illustration of the computation model is shown in Fig. 3. Four observation points are indicated in Fig. 4 at the locations of A, B, C, and D. Their distances to the track centerline are 0, 6.25, 11.25, and 21.25 m, respectively. Table 1 shows the parameters of the train, and Table 2 shows the parameters of the track structure and ground.

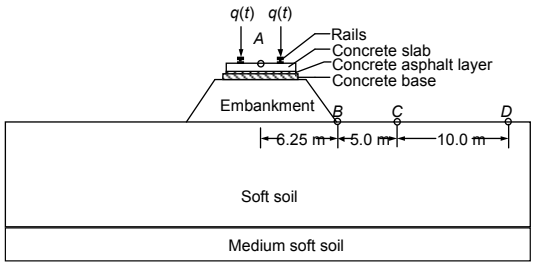

Fig. 3 Transverse section of the track and ground (not to scale)

Table 1 Parameters for vehicle model

Parameter	Value	Parameter	Value
m_c (kg)	4240	c_p (N/m)	5.00×10^3
m_b (kg)	3400	k_s (N/m)	4.00×10^5
m_w (kg)	2200	c_s (N/m)	6.00×10^3
k_p (N/m)	1.04×10^6		

4.1 Effect of amplitude of track irregularities on dynamic responses

The wavelength of the track vertical irregularity usually lies within the range 0.125–14 m, which can be divided into short wavelength and long wavelength zones. In this study, two typical wavelengths, L=0.5 m and 10.0 m, are chosen to be analyzed. Two typical train speeds are chosen, c=50 m/s and 100 m/s, respectively. In this track-ground model, the shear wave velocity of the upper soft soil is 81.1 m/s, and the train running at high speed can exceed it easily. Three amplitudes of the track irregularities are chosen, A_r=0 mm, 3 mm, and 10 mm. The ground vibration induced by a train passing a track with irregularity wavelength L=0.5 m and 10 m at speed c=50 m/s are presented in Fig. 4 and Fig. 5, respectively. For the train running at high-speed c=100 m/s, the computation results presented in Fig. 6 and Fig. 7 for wavelength of irregularities at L=0.5 m and 10 m, respectively.

From Figs. 4 and 5, it is seen that dynamic responses both at track and on ground increase monotonically with the irregularity amplitude. Compared to the smooth track, A_r=0 mm, the track irregularities have significant impact on track and ground vibration, especially at a further distance from the track center. The comparison of the results in Figs. 4 and 5 indicates that long wavelength irregularities generate low frequency vibration, which attenuates slowly in more distant ground. Finally, the vibration intensity

Table 2 Parameters of the track and ground

Material	Poisson's ratio	Density (kg/m^3)	Thickness (m)	Damping ratio	Elastic modulus (MPa)
Concrete slab	0.20	2500	0.20	0.05	24000
Concrete asphalt mortar	0.30	1800	0.05	0.20	100
Concrete base	0.20	2400	0.30	0.05	10000
Embankment	0.36	1400	3.00	0.05	170
Soft soil	0.47	1550	15.0	0.05	30
Medium soft soil	0.49	1750	5.00	0.05	116

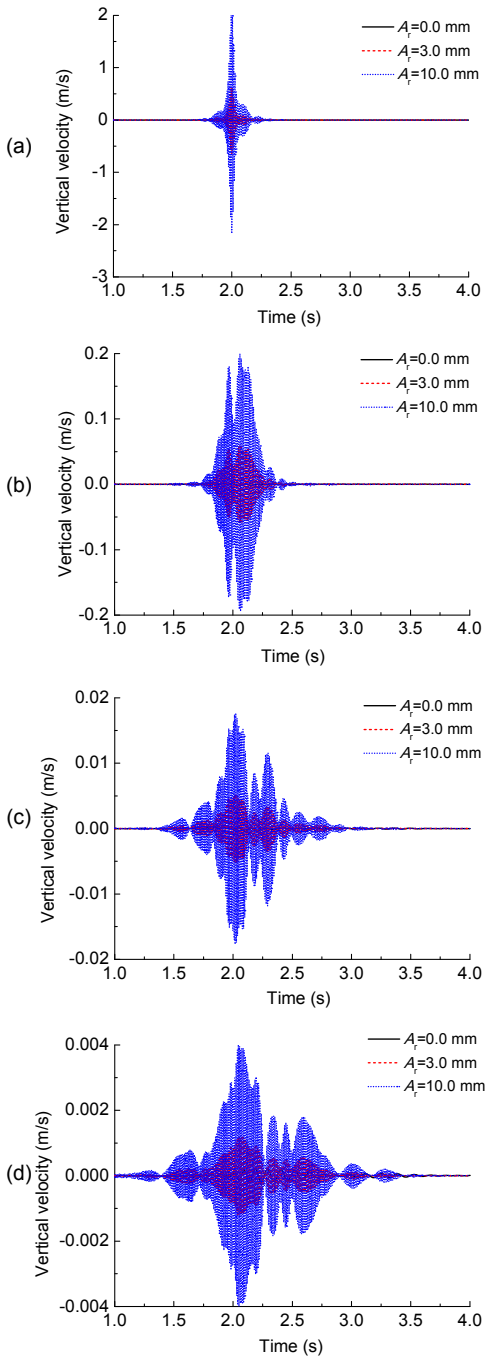

Fig. 4 Vertical velocity responses for conditions of L=0.5 m and c=50 m/s

(a) Point A at track center; (b) Point B at y=6.25 m; (c) Point C at y=11.25 m; (d) Point D at y=21.25 m

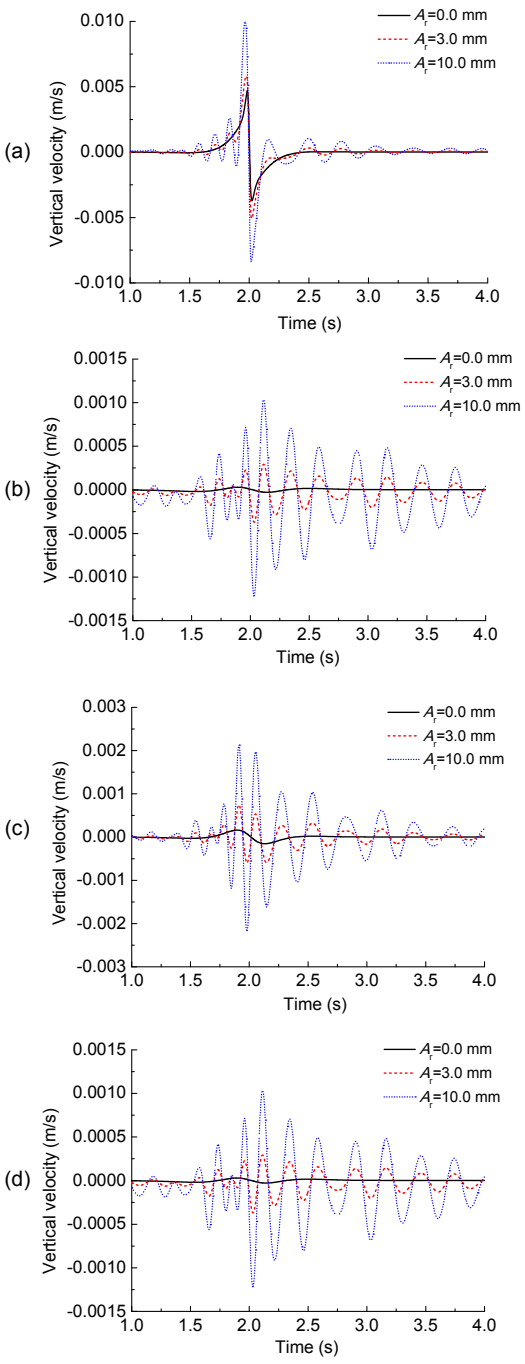

Fig. 5 Vertical velocity responses for conditions of L=10.0 m and c=50 m/s

(a) Point A at track center; Point B at y=6.25 m; (c) Point C at y=11.25 m; (d) Point D at y=21.25 m

at the embankment toe is about 10% of that at the track center, which means that the embankment effectively reduces the vibration transmission to adjacent ground.

From Figs. 6 and 7, it is interesting to note that when train's running speed surpasses the critical velocity of the track-ground system (the Rayleigh wave velocity of the upper soft soil layer), track and ground

vibrations show different features compared to a slow-speed train. For the track with short wavelength irregularities, track vibrations generated are still dominated by high-frequency responses due to track irregularities, but at a further distance, vibration generated by train's wheel axle weights becomes dominant. In sharp contrast, for the track with long wavelength irregularities, both track and ground vibrations are produced by the movement of train's wheel axle weights. There is very little difference between the vibrations generated by train running on smooth track or track with irregularities.

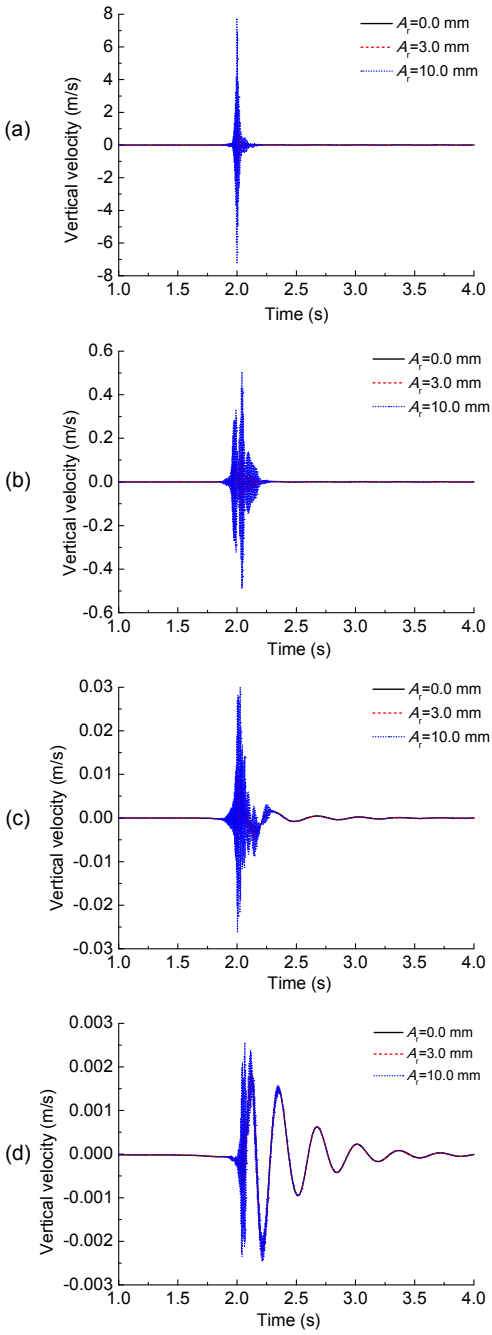

Fig. 6 Vertical velocity responses for conditions of L=0.5 m and c=100 m/s

(a) Point A at track center; (b) Point B at y=6.25 m; (c) Point C at y=11.25 m; (d) Point D at y=21.25 m

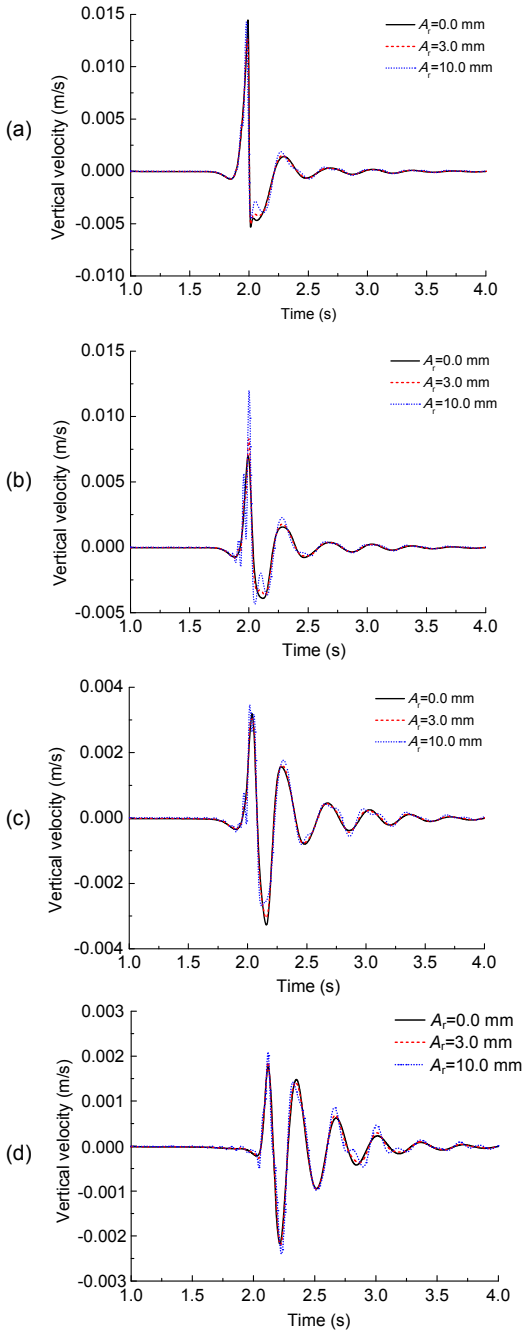

Fig. 7 Vertical velocity responses for conditions of L=10.0 m and c=100 m/s

(a) Point A at track center; (b) Point B at y=6.25 m; (c) Point C at y=11.25 m; (d) Point D at y=21.25 m

The comparisons among Fig. 4 and Fig. 6, and Fig. 5 and Fig. 7 show that, generally, short wavelength irregularities generate more significant ground vibrations than the longer ones.

To explore the vibration attenuation mechanism with the distance from track center, the following definition is adopted:

$$H = 20\lg\left(\frac{V}{V_0}\right), \tag{14}$$

where V is the amplitude of actual vibration velocity, and V_0 is the reference value with amplitude of 10^{-8} m/s.

As mentioned above, two typical wavelengths are chosen to investigate the influence of track irregularity upon the vibration intensities due to train running. The computation results are presented in Figs. 8 and 9 for train speeds at 50 and 100 m/s, respectively.

Fig. 8 shows the variation of vertical vibration intensity with distance from track center for train speed c=50 m/s. From the computation results, it is found that the irregularity amplitude has sharp impact on the vertical response intensity for low-speed train, both for short wavelength and long wavelength irregularities. However, there are still some differences for these two cases. For short wavelength case, the vibration curves are parallel to each other with the distance increase; however, for long wavelength case, the vibration curves divergence increase gradually with the distance. Especially for the long wavelength case, there is vibration amplification at distance about 27 m from the track center, while for the short wavelength case, ground vibration intensity decreases almost monotonically with distance from track center.

Fig. 9 shows the variation of vertical vibration intensity with distance from track center for train speed c=100 m/s. These results show that the irregularity amplitude has a sharp impact on the vertical vibration intensity at ground adjacent to the track for short wavelength case. However, this is not obvious for the long wavelength case and at the ground distant from the track center.

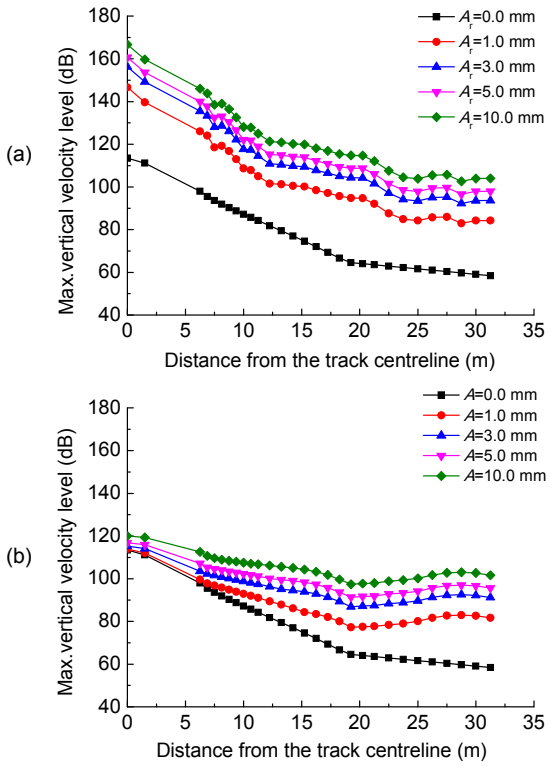

Fig. 8 Variation of vertical vibration intensity with distance from track center for train speed c=50 m/s

(a) L=0.5 m; (b) L=10 m

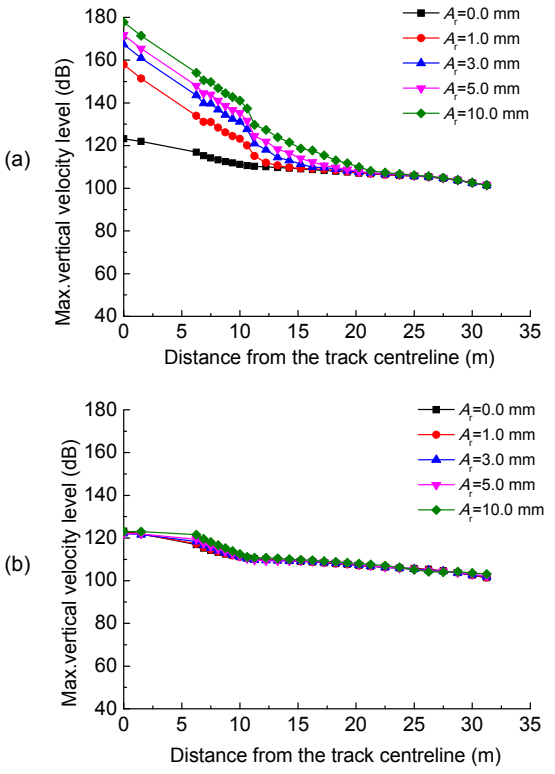

Fig. 9 Variation of vertical vibration intensity with distance from track center for train speed c=100 m/s

(a) L=0.5 m; (b) L=10 m

4.2 Effect of wavelength of track irregularities on dynamic responses

The influence of irregularity wavelength on vibration under c=50 m/s and c=100 m/s are shown in Fig. 10. In this section, the irregularity amplitude is fixed as 3 mm. Fig. 10 shows that the track irregularity with shorter wavelength can generate stronger track vibration both for low-speed and high-speed cases. However, when train runs at a low speed, vibration induced by track irregularities can be transmitted over a long distance. When a train runs at high-speed, the wavelength of track irregularities has very little effect on ground vibration at further distances from the track center. Therefore, it can be concluded that the ground vibration further away from the track is dominated by low frequency vibration.

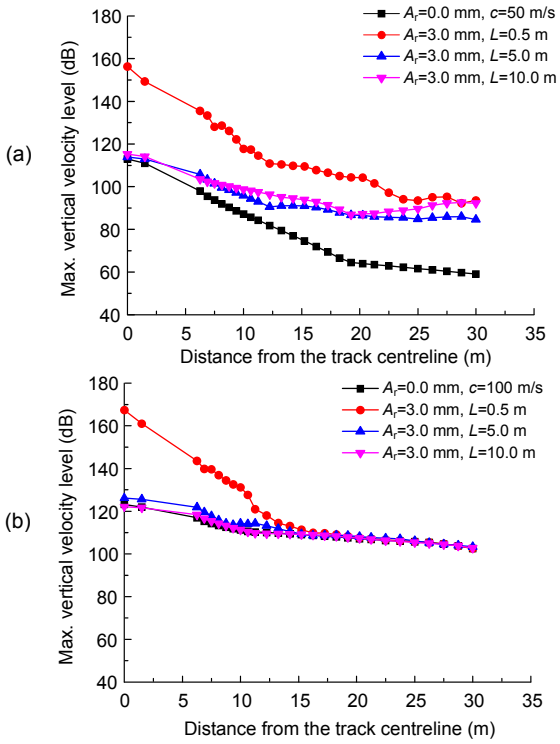

Fig. 10 Influence of track irregularity wavelength on ground vibration

(a) c=50 m/s; (b) c=100 m/s

4 Conclusions

In this paper, the track irregularities and one-quarter car model are coupled into the 2.5D finite element model of track and ground. The effects of track irregularities on the track and ground vibrations are discussed. The wave motions at ground surface due to a train running at different speeds are also presented. The following conclusions are made by parametric analyses.

Two main parameters of track irregularities, amplitude and wavelength, have crucial influences on track and ground vibrations, but they operate via different mechanisms. The irregularity amplitude has a direct impact on the vertical response for low-speed trains, both for short wavelength and long wavelength irregularities. Track irregularity with shorter wavelength can generate stronger track vibration both for low-speed and high-speed cases. For low-speed case, vibrations induced by track irregularities dominate far field responses. For high-speed case, the wavelength of track irregularities has very little effect on ground vibration at distances far from track center.

When train's running speed is close to the critical velocity of the track-ground system, track and ground vibrations show different features. For the short wavelength track irregularities case, track vibrations generated are dominated by high-frequency responses due to track short wavelength irregularities, while at further distances, ground vibration generated by train's wheel axle weights becomes dominant. For the track with long wavelength irregularities, both track and ground vibrations are produced by the movement of the train's wheel axle weights. There is very little difference between the vibrations generated by trains running on a smooth track or a track with irregularities.

References

Adolfsson, K., Andreasson, B., Bengtson, P.E., Bodare, A., Madshus, C., Massarch, R., Wallmark, G., Zackrisson, P., 1999. High Speed Lines on Soft Ground. Evaluation and Analysis of Measurements from the West Coast Line. Technical Report, Banverket, Sweden.

Auersch, L., 2005. The excitation of ground vibration by rail traffic: theory of vehicle-track-soil interaction and measurements on high-speed lines. *Journal of Sound and Vibration*, **284**(1-2):103-132. [doi:10.1016/j.jsv.2004.06.017]

Bian, X.C., Chen, Y.M., Hu, T., 2008. Numerical simulation of high-speed train induced ground vibrations using 2.5D finite element approach. *Science in China Series G: Physics Mechanics and Astronomy*, **51**(6):632-650. [doi:10.1007/s11433-008-0060-3]

Degrande, G., Lombaert, G., 2001. An efficient formulation of Krylov's prediction model for train induced vibrations based on the dynamic reciprocity theorem. *Journal of the*

Acoustical Society of America, **110**(3):1379-1390. [doi:10.1121/1.1388002]

Galvin, P., Dominguez, J., 2007. High-speed train-induced ground motion and interaction with structures. *Journal of Sound and Vibration*, **307**(3-5):755-777. [doi:10.1016/j.jsv.2007.07.017]

Galvin, P., Françoisa, S., Schevenelsa, M., Bonginic, E., Degrandea, G., Lombaerta, G., 2010a. A 2.5D coupled FE-BE model for the prediction of railway induced vibrations. *Soil Dynamics and Earthquake Engineering*, **30**(12):1500-1512. [doi:10.1016/j.soildyn.2010.07.001]

Galvin, P., Romero, A., Dominguez, J., 2010b. Fully three-dimensional analysis of high-speed train-track-soil-structure dynamic interaction. *Journal of Sound and Vibration*, **329**(24):5147-5163. [doi:10.1016/j.jsv.2010.06.016]

Heckl, M., Hauck, G., Wettschureck, R., 1996. Structure-borne sound and vibration from rail traffic. *Journal of Sound and Vibration*, **193**(1):175-184. [doi:10.1006/jsvi.1996.0257]

Katou, M., Matsuoka, T., Yoshioka, O., Sanada, Y., Miyoshi, T., 2008. Numerical simulation study of ground vibrations using forces from wheels of a running high-speed train. *Journal of Sound and Vibration*, **318**(4-5):830-849. [doi:10.1016/j.jsv.2008.04.053]

Krylov, V.V., 1995. Generation of ground vibration by superfast trains. *Applied Acoustics*, **44**(2):149-164. [doi:10.1016/0003-682X(95)91370-I]

Lombaert, G., Degrande, G., 2009. Ground-borne vibration due to static and dynamic axle loads of InterCity and high-speed trains. *Journal of Sound and Vibration*, **319**(3-5):1036-1066. [doi:10.1016/j.jsv.2008.07.003]

Rigueiro, C., Rebelo, C., Da Silva, L.S., 2010. Influence of ballast models in the dynamic response of railway viaducts. *Journal of Sound and Vibration*, **329**(15):3030-3040. [doi:10.1016/j.jsv.2010.02.002]

Sheng, X., Jones, C., Petyt, M., 1999a. Ground vibration generated by a harmonic load acting on a railway track. *Journal of Sound and Vibration*, **225**(1):3-28. [doi:10.1006/jsvi.1999.2232]

Sheng, X., Jones, C., Petyt, M., 1999b. Ground vibration generated by a load moving along a railway track. *Journal of Sound and Vibration*, **228**(1):129-156. [doi:10.1006/jsvi.1999.2406]

Sheng, X., Jones, C., Thompson, D.J., 2003. A comparison of a theoretical model for quasi-statically and dynamically induced environmental vibration from trains with measurements. *Journal of Sound and Vibration*, **267**(3):621-635. [doi:10.1016/S0022-460X(03)00728-4]

Sheng, X., Jones, C., Thompson, D.J., 2004. A theoretical model for ground vibration from trains generated by vertical track irregularities. *Journal of Sound and Vibration*, **272**(3-5):937-965. [doi:10.1016/S0022-460X(03)00782-X]

Takemiya, H., 2003. Simulation of track-ground vibrations due to a high-speed train: The case of X-2000 at Ledsgard. *Journal of Sound and Vibration*, **261**(3):503-526.

Takemiya, H., Bian, X.C., 2005. Substructure simulation of inhomogeneous track and layered ground dynamic interaction under train passage. *Journal of Engineering Mechanics*, **131**(7):699-711. [doi:10.1061/(ASCE)0733-9399(2005)131:7(699)]

Yang, B.Y., Hung, H.H., 2001. A 2.5D finite/infinite element approach for modelling visco-elastic bodies subjected to moving loads. *International Journal for Numerical Methods in Engineering*, **240**:1317-1336. [doi:10.1002/nme.208]

2010 JCR of Thomson Reuters for *JZUS-A* and *JZUS-B*

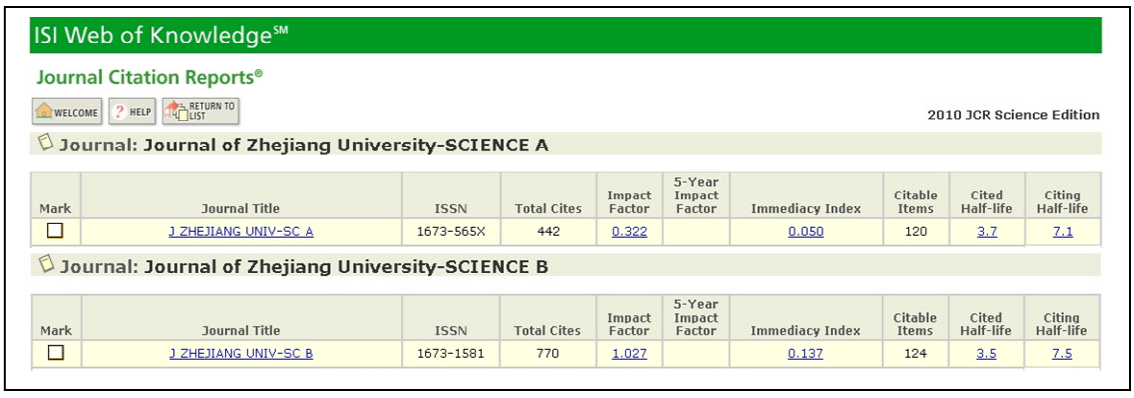

ISI Web of Knowledge℠

Journal Citation Reports®

WELCOME HELP RETURN TO LIST

2010 JCR Science Edition

Journal: Journal of Zhejiang University-SCIENCE A

Mark	Journal Title	ISSN	Total Cites	Impact Factor	5-Year Impact Factor	Immediacy Index	Citable Items	Cited Half-life	Citing Half-life
☐	J ZHEJIANG UNIV-SC A	1673-565X	442	0.322		0.050	120	3.7	7.1

Journal: Journal of Zhejiang University-SCIENCE B

Mark	Journal Title	ISSN	Total Cites	Impact Factor	5-Year Impact Factor	Immediacy Index	Citable Items	Cited Half-life	Citing Half-life
☐	J ZHEJIANG UNIV-SC B	1673-1581	770	1.027		0.137	124	3.5	7.5